Electronic structure of indium oxide using cluster calculations

Isao Tanaka, Masataka Mizuno, and Hirohiko Adachi

Department of Materials Science and Engineering, Kyoto University, Sakyo, Kyoto 606-01, Japan

We report first-principles electronic-structure calculations of In_2O_3 using the discrete variational $X\alpha$ method on model clusters. The computation has been made up to the model cluster composed of 163 atoms in order to see the size effect. The In-O bond is found to be predominant in In_2O_3, and both O-O and In-In bonds are much weaker. Antibonding interaction between O-$2p$ with nearly filled In-$4d$ orbitals near the top of the valence band is noticed. Valence-band structure by XPS is well reproduced by the calculation. Unoccupied In-$5sp$ orbitals show wide spatial distribution over the third In shell. Direct interaction between In-$5sp$ orbitals is found to be important in the excited states. When an oxygen vacancy is present, a vacancy level appears in between the band gap. The vacancy level is composed of In-$5sp$ orbitals hybridized with O-$2p$ orbitals, which exhibits a strong In-In bonding interaction. The occupation of the vacancy level due to the localization of electrons to the oxygen vacancy thus results in the reinforcement of the In-In bond strength. This is suggested to be the electronic mechanism for the stability of the oxygen vacancies in the In_2O_3 crystal. [S0163-1829(97)05531-8]

Indium oxide film has been widely used for transparent electrodes of solar cells, display devices, etc. Since the properties of these films are sensitively changed by small amount of dopants and their preparation conditions, a number of studies have been made to optimize the processing parameters.[1] However, only a few of these engineering works have been published; we still do not share much common knowledge as guiding principles for the materials/processing design of these materials.

Fan and Goodenough[2] built up a schematic energy-band model for Sn-doped In_2O_3 (indium-tin oxide; ITO) on the basis of their extensive x-ray photoemission spectroscopy studies. Optical properties of In_2O_3 were investigated by several groups. Most of these works showed that the energy gap of In_2O_3 was about 3.7 eV.[1] However, no first-principles calculation of the electronic structure of In_2O_3 has thus far been reported. The theoretical band structure by empirical tight-binding method[3] is the only available one. It is not accidental, since In_2O_3 exhibits a complicated crystal structure having 80 atoms in a unit cell. Heavy elements like In are difficult to treat by first-principles calculation in general unless core orbitals are removed from the diagonalization to solve the secular equation. It is therefore a purpose of this paper to elucidate the electronic structure of undoped In_2O_3 as well as its chemical bonding mechanism. Cluster size dependence of the electronic structure is systematically investigated, because we are interested in the spatial distribution of each atomic orbital in In_2O_3. The size dependence is also of great interest from the viewpoint of materials science, since we are able to synthesize nanocrystalline ceramic materials through modern experimental techniques. The ultrafine particles often exhibit peculiar properties to its size.

Indium oxide has a C-type rare-earth structure (space group Ia3, No. 206) similar to many trivalent rare-earth oxides, such as Yb_2O_3 and Dy_2O_3. They are composed of eight fluorite-type unit cells with systematic anion vacancies. The unit cell is composed of 8 In(1) atoms at the b site, 24 In(2) atoms at the d site, and 48 oxygen atoms at the e sites according to the Wyckoff's notation. The lattice parameter of the cubic cell is 10.117 Å. All In atoms are coordinated by six oxygens forming a distorted octahedron. The bond length of In-O is ranged from 2.12 to 2.21 Å. The neighboring octahedra are shared with their corners and edges. The sublattice of In is close to the fcc (face-centered cubic) structure; All In atoms are surrounded by 12 In atoms in the In sublattice. The In-In distance is ranging from 3.35 to 3.36 Å, where the edges of the neighboring InO_6 octahedra are shared. It is ranging from 3.82 to 3.84 Å where the octahedra are corner shared.

Atomic clusters used for the molecular-orbital (MO) calculation were two types of $(InO_6)^{9-}$ clusters centered at two different crystallographic sites, $(In_4O_{17})^{22-}$ cluster, $(In_{13}O_{42})^{45-}$ cluster, $(In_{19}O_{60})^{63-}$ cluster, and $(In_{43}O_{120})^{111-}$ cluster. Since the In-sublattice is close to the fcc structure, the $(In_{13}O_{42})^{45-}$ cluster includes 12 first-nearest-neighbor In ions from the In ion at the center of the cluster. The $(In_{19}O_{60})^{63-}$ and $(In_{43}O_{120})^{111-}$ clusters include the second and third-nearest-neighbor In ions, respectively. All clusters are embedded in Madelung potential generated by point charges outside the cluster. Convergence of the direct sum of the Madelung potential with respect to monopole and dipole sum[4] was found to be achieved within the accuracy of 10^{-4}.

Nonrelativistic first-principles MO calculations were made by the discrete-variational (DV)-$X\alpha$ method[5,6] using a program code SCAT.[6] MO were constructed by linear combination of atomic orbitals (AO) as

$$\phi_l(r_k) = \sum_i C_{il}\chi_i(r_k), \tag{1}$$

where $\chi_i(r)$ denotes the AO, and r_k is one of the sampling points in the DV calculation. The number of the sampling points was chosen to be 1400 per atom. The total number of the sampling points over the cluster was therefore 2.3×10^5 for the $(In_{43}O_{120})^{111-}$ cluster. The numerical basis functions were obtained by solving the radial part of the Schrödinger equations. Minimal basis sets, i.e., $1s-2p$ for O and $1s-4d$, $5s$, $5p$ for In are used.

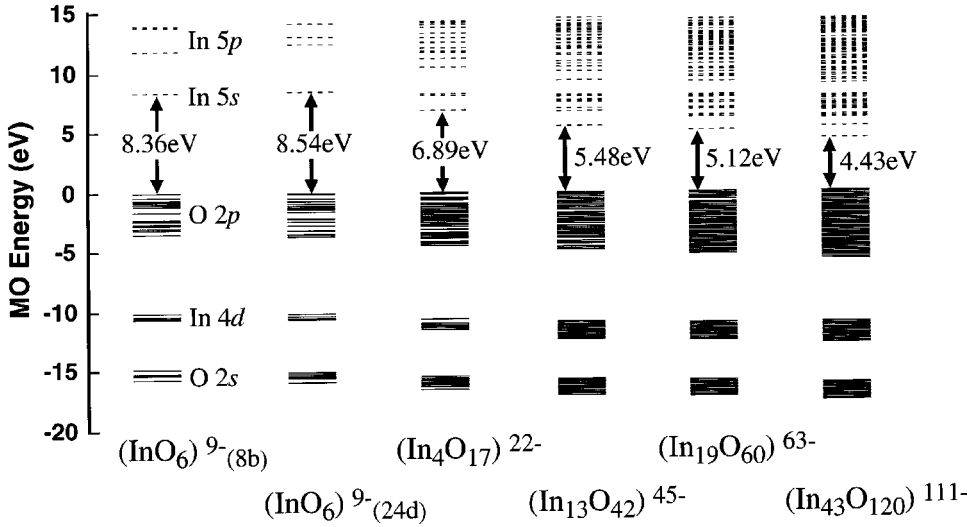The overlap population between ith AO and jth AO at the lth MO is given by

FIG. 1. Energy eigenvalues for six clusters.

$$Q_{ij}^l = C_{il} C_{jl} \sum_k \omega(r_k) \chi_i(r_k) \chi_j(r_k), \qquad (2)$$

where $\omega(r)$ is the integration weight or reciprocal of the sample point density at r_k. The sum of Q_{ij}^l with respect to l for occupied orbitals provides the net overlap population between i th AO and jth AO, i.e.,

$$Q_{ij} = \sum_l^{\text{occupied}} Q_{ij}^l. \qquad (3)$$

The overlap population between atom A and B is given by

$$Q_{AB}^l = \sum_{i \in A} \sum_{j \in B} Q_{ij}^l. \qquad (4)$$

Overlap-population diagrams are made by broadening of Q_{AB}^l at individual MOs using Gaussian functions of 1.0-eV full width at half maximum (FWHM). The orbital population of the ith orbital is given by

$$Q_i = \sum_l^{\text{occupied}} \sum_j Q_{ij}^l. \qquad (5)$$

The net charge of each atom ΔQ_A is obtained by

$$\Delta Q_A = Z_A - \sum_{i \in A} Q_i, \qquad (6)$$

where Z_A is the atomic number of atom A.

Figure 1 shows the MO eigenvalues obtained for six kinds of clusters. MO energies are aligned so as to make the highest occupied MO (HOMO) zero. Solid lines and broken lines denote occupied and unoccupied levels, respectively. As can be seen, the framework electronic structures are not significantly dependent on the cluster size. Only the width of each band is broadened with rising cluster size because of the inclusion of the non-nearest-neighbor interactions. Fan and Goodenough[2] made a schematic energy-band model for In_2O_3. They showed that the In-$4d$ band overlaps with the bottom of the O-$2p$ band. Contrary to their model, we found that the In-$4d$ band is located in between O-$2s$ and O-$2p$ bands.

The band gap between the highest occupied MO (HOMO) and the lowest unoccupied MO (lowest unoccupied molecular orbital) decreases with rising the cluster size, and it does not converge at our largest cluster which includes third In shells from the central In ion. The width of the unoccupied In-$5sp$ band shows a similar size dependence to that of the band gap in the opposite sign. The major origin of the size dependence of the band gap can therefore be ascribed to that of the unoccupied In-$5sp$ band, although the size dependence of the O-$2p$ band width is partly responsible. The present result implies that the spatial distribution of the In-$5sp$ band is greater than the third-nearest-neighbor In-In distance. In other words, the In-$5sp$ orbitals directly interact with other orbitals within the third In shells.

Figure 2 displays total and partial density of states (DOS) obtained for the largest cluster, $(In_{43}O_{120})^{111-}$. All of these curves are made by broadening the discrete energy eigenvalues by Gaussian functions of 0.5-eV FWHM. A small contribution of In-$4d$, $5s$, and $5p$ orbitals in O-$2s$ and O-$2p$ bands can be recognized. The presence of In-$5s$ and $5p$ orbitals in the O-$2p$ band is natural for ionic compounds with partial covalency. However, the hybridization of the filled In-$4d$ orbital with O-$2s$ and O-$2p$ orbitals is noteworthy.

The DOS curves shown in Fig. 2 may be useful for assignments of spectral features obtained by electron spectroscopies, such as x-ray photoemission, x-ray-absorption, x-ray emission, electron-energy-loss spectroscopy, etc. Figure 3 compares the experimental x-ray photoemission spectrum (XPS) reported by Barr and Liu[7] with the theoretical XPS spectrum obtained from the DOS curves shown in Fig. 2. Although the incident x-ray energy was not specified in Ref. 7, we have assumed the Al-$K\alpha$ radiation, and the partial photoionization cross sections for individual atomic orbitals were taken from literature.[8] Since the partial photoionization cross section for In-$5p$ orbital was not tabulated, it was assumed to be 8×10^{-4} that is the value for Sn-$5p$. Since the partial photoionization cross section of In-$4d$ is 130 times greater than that of O-$2p$, the XPS at the valence band strongly reflects the structure of the In-$4d$ partial DOS in the valence band. As can be seen in Fig. 3, the theoretical XPS well reproduces the experimental one except for the intensity
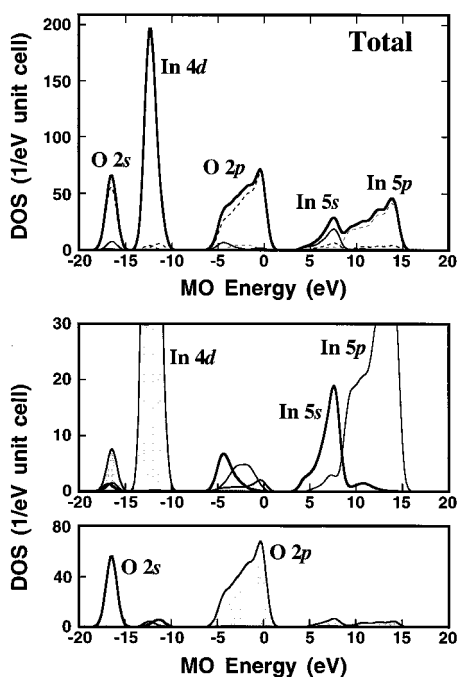
FIG. 2. Density of states calculated for the $(In_{43}O_{120})^{111-}$ cluster and its partial components.

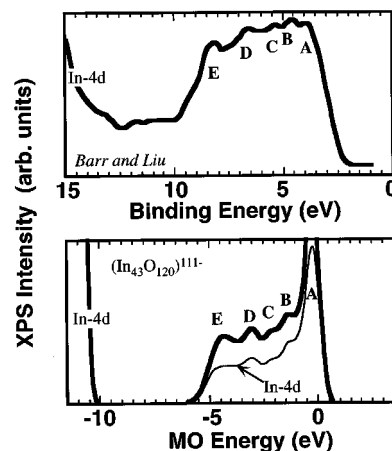FIG. 3. Theoretical XPS calculated for the $(In_{43}O_{120})^{111-}$ cluster in comparison with the experimental spectrum in Ref. 7. In-$4d$ component for the theoretical XPS is shown together.

of the peak A. The disagreement may be ascribed to the overestimation of the partial photoionization cross section of In-$4d$ for the In_2O_3 crystal. It should be smaller by a factor of 4.

Mulliken's population analysis found that the bonding of In_2O_3 does not fit the fully ionic picture. Net charges evaluated for the $(In_{43}O_{120})^{111-}$ cluster are $+2.03$ for In and -1.65 for O, respectively. There should be a small covalent bonding between In and O. Overlap-population diagrams for In-O, In-In, and O-O bonds obtained for the $(In_{43}O_{120})^{111-}$ cluster are shown in Fig. 4. The right part of each diagram shows the bonding contribution and the left part shows the antibonding contribution. The integration of both bonding and antibonding contributions up to the highest occupied MO (HOMO) provides the bond-overlap population for each bond. These values show that the major bonding mechanism of the ideal In_2O_3 crystal is the covalent bond of the In-O.

Regarding the In-O interaction, the O-$2s$ band $(-15--17$ eV) is completely bonding. The In-4d band $(-10--12$ eV) displays both bonding and antibonding contributions for almost the same amount. The major part of the O-$2p$ band $(0--5$ eV) shows a bonding contribution. However, there is an antibonding contribution due to the interaction between O-$2p$ and In-$4d$ orbitals near the top of the valence band.

The O-O bond is less significant than the In-O bond. The balance of the bonding and anitbonding contributions in all of the O-$2s$, $2p$, and In-$4d$ bands makes the net bond-overlap population a small negative value. The In-In interaction is much weaker than the other two kinds of bonds. There are two groups of In-In distances depending upon the manner of the InO_6 octahedral linkage in the In_2O_3 crystal. It is around 3.36 Å when the neighboring octahedra are edge shared, and around 3.83 Å when they are corner shared. Irrespective of the linkage, the direct In-In covalent bond is found to be weak. It should be noted, however, the overlap population between In orbitals is strong in the unoccupied band where the In-$5sp$ orbitals are dominant. Although they play little role in the chemical bonding of the ideal In_2O_3 at the ground state, the In-In interaction becomes important at the excited states as well as doped or defective crystals where these higher-energy states are partially occupied by electrons.
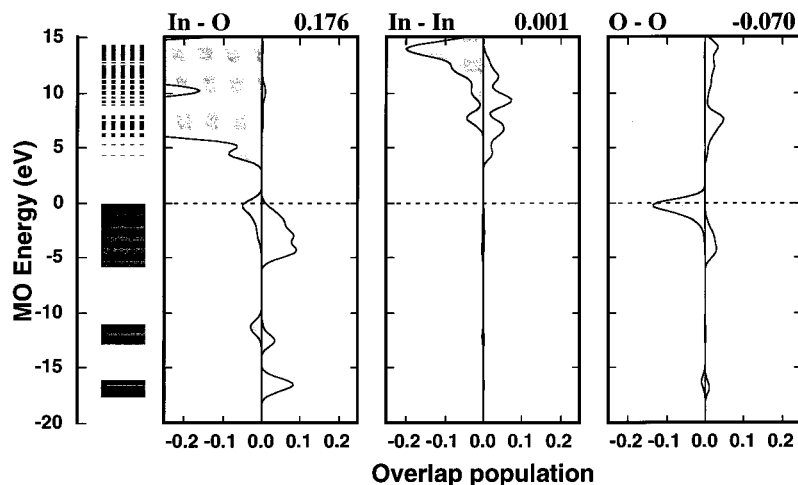

FIG. 4. Overlap-population diagrams for the $(In_{43}O_{120})^{111-}$ cluster. The value shown on the top of each diagram is the bond-overlap population for the corresponding bond.

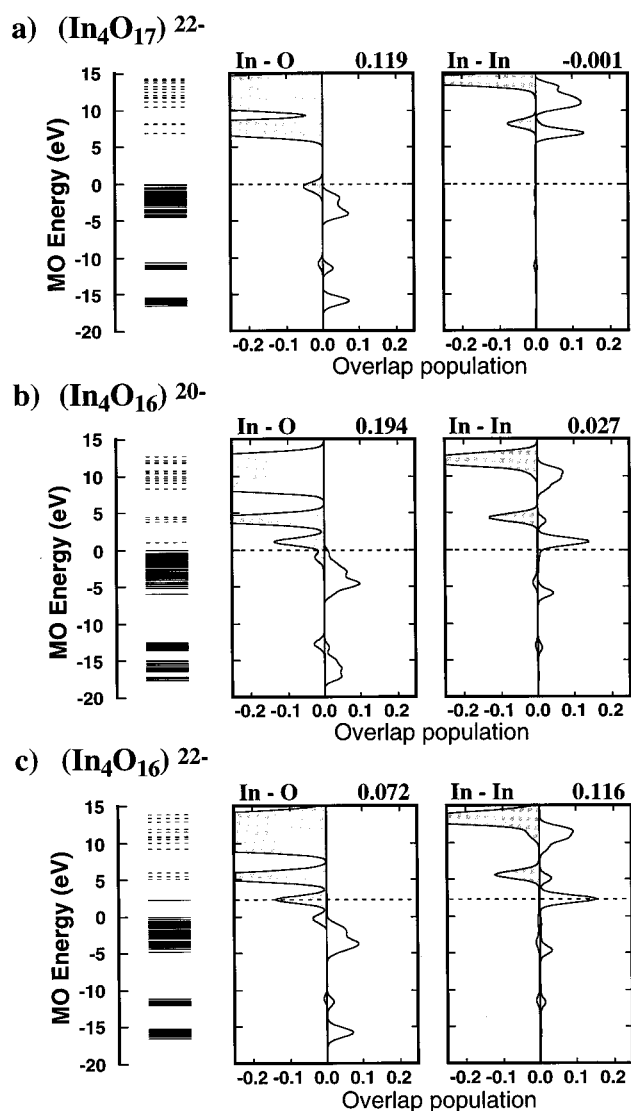**a) $(In_4O_{17})^{22-}$**

b) $(In_4O_{16})^{20-}$

c) $(In_4O_{16})^{22-}$

FIG. 5. Overlap-population diagrams for $(In_4O_{17})^{22-}$, $(In_4O_{16})^{20-}$, and $(In_4O_{16})^{22-}$ clusters.

Doubly ionized oxygen vacancies, $V_{\ddot{O}}$, have been considered to be the predominating point defects in In_2O_3 through the analysis of the dependence of the oxygen partial pressure on the electrical conductivity under thermal equilibrium conditions.[9] Since the oxygen vacancies should play important roles for electronic/optical properties of In_2O_3, the electronic states associated with the oxygen vacancies are of great interest.

The electronic states of a model cluster that contains an oxygen vacancy are calculated. For this purpose, a cluster that has an oxygen at the center, i.e., $(In_4O_{17})^{22-}$ cluster, is used. The top panel of Fig. 5 displays the MO level structure and overlap-population diagram of the $(In_4O_{17})^{22-}$ cluster. Comparison of the overlap-population diagram with that of the $(In_{43}O_{120})^{111-}$ cluster shown in Fig. 4 finds that the framework structures of diagrams are the same except for a small difference in the unoccupied In-$5sp$ band. The $(In_4O_{16})^{20-}$ cluster and the $(In_4O_{16})^{22-}$ cluster contain a doubly ionized and neutral oxygen vacancy at the center of the $(In_4O_{17})^{22-}$ cluster, respectively. Results for these two clusters are shown together in Fig. 5.

When a doubly ionized oxygen vacancy, $V_{\ddot{O}}$, is present, two phenomena can be noticed: (1) Decrease in the energy of the In-$5sp$ bands by 3 eV, and (2) formation of a discrete level in between the band gap. The shape of the overlap-population diagrams is not significantly altered by the presence of the vacancy. It is simply shifted in energy. However, the discrete level that is newly appeared is strong antibonding for the In-O and strong bonding for the In-In interaction. This level will be hereafter called the vacancy level. When two extra electrons are put into the $(In_4O_{16})^{20-}$ cluster to model the neutral oxygen vacancy, the vacancy level is fully occupied; the chemical bonding around the vacancy is therefore remarkably changed. When a doubly ionized vacancy is present, the overlap population between In and O is reinforced in exchange for the loss of the number of bonds. The In-In bond is not notably altered in this case. On the other hand, the In-O bond is significantly weakened when electrons are localized at the vacancy because of the occupation of the antibonding level. At the same time, the In-In bond is reinforced remarkably. The electronic mechanism behind the abundance of the oxygen vacancy in the In_2O_3 crystal can therefore be ascribed to the formation of the In-In bond around the vacancy.

[1] Z. M. Jarzebski, Phys. Status Solidi A **71**, 13 (1982).

[2] J. C. C. Fan and J. B. Goodenough, J. Appl. Phys. **48**, 3524 (1977).

[3] E. A. Albanesi, S. J. Sferco, I. Lefebvre, G. Allan, and M. Lannoo, Solid State Commun. **86**, 27 (1993).

[4] H. Coker, J. Phys. Chem. **87**, 2512 (1983).

[5] H. Adachi, M. Tsukada, and C. Satoko, J. Phys. Soc. Jpn. **45**, 875 (1978).

[6] D. E. Ellis, H. Adachi, and F. W. Averill, Surf. Sci. **58**, 497 (1976).

[7] T. L. Barr and Y. L. Liu, J. Phys. Chem. Solids **50**, 657 (1989).

[8] J. J. Yeh and I. Lindau, At. Data Nucl. Data Tables **32**, 1 (1985).

[9] J. H. W. de Wit, G. van Unen, and M. Lahey, J. Phys. Chem. Solids **38**, 819 (1977).